

Adaptive Space Warping to Enhance Passive Haptics in an Arthroscopy Surgical Simulator

Jonas Spillmann, Stefan Tuchschmid, and Matthias Harders

Abstract—Passive haptics, also known as tactile augmentation, denotes the use of a physical counterpart to a virtual environment to provide tactile feedback. Employing passive haptics can result in more realistic touch sensations than those from active force feedback, especially for rigid contacts. However, changes in the virtual environment would necessitate modifications of the physical counterparts. In recent work space warping has been proposed as one solution to overcome this limitation. In this technique virtual space is distorted such that a variety of virtual models can be mapped onto one single physical object. In this paper, we propose as an extension adaptive space warping; we show how this technique can be employed in a mixed-reality surgical training simulator in order to map different virtual patients onto one physical anatomical model. We developed methods to warp different organ geometries onto one physical mock-up, to handle different mechanical behaviors of the virtual patients, and to allow interactive modifications of the virtual structures, while the physical counterparts remain unchanged. Various practical examples underline the wide applicability of our approach. To the best of our knowledge this is the first practical usage of such a technique in the specific context of interactive medical training.

Index Terms—Virtual reality, passive haptics, surgical training simulation

1 INTRODUCTION

The sense of touch is an intrinsically important feature in surgical simulators [7]. Haptic feedback significantly eases the navigation inside the virtual environment (VE) as users are kept from passing through apparently solid virtual surfaces. This directly increases the level of immersion [15], and thus affects the training outcome. Usually, the physical contact forces are provided by a haptic device. However, including haptic feedback can be expensive – both from a commercial and a computational point-of-view, especially if rigid contacts must be handled.

The concept of *passive haptics*, also known as *tactile augmentation* or *mixed reality*, provides a cost-effective alternative to active haptic feedback. It denotes the addition of real physical objects into the VE, resulting in compelling tactile sensations. However, the mapping between the VE and the associated physical objects (also denoted as *props*) is usually one-to-one, which makes the VE inflexible. Especially in the context of surgical simulators, employing passive haptics leads to difficulties, since changes in the simulation or differing virtual cases cannot easily be represented.

An obvious way to overcome this limitation is by allowing some discrepancy in the mapping between the virtual and the physical objects. In order to accomplish this, the virtual space can be warped, resulting in a difference between the motion of the user-guided instrument in the real and the virtual world [20, 2]. To give an example, consider a tool displaced with constant velocity on a flat, real planar object. Using the described techniques, this geometry can be mapped to a curved surface in the VE. As a consequence, the path of the corresponding visual avatar in the VE is warped. Also, the velocity does not remain constant in order to maintain a coherent sensation during the movement (see Fig. 1). In [20] it is also indicated that space warping has the potential to increase the number of training cases.

In this paper, we build upon the previous research and show how the concept of static space warping can be extended to accommodate dynamically changing simulations. We illustrate our methods in the context of a training simulator for knee arthroscopy. Virtual patients differing in the shapes of their bones are mapped to one generic anatomical hardware. In addition, our method also allows the representation of differences in the mechanical behavior of the knee joints. A strength of our approach is that the mapping from the virtual to the real world can be temporally varying, thus accommodating the interactive modification of anatomical structures. This is particularly important in the context of surgical resection, for instance in our test-bed the removal of damaged parts of the knee menisci (*meniscectomy*). Both the mapping of the mechanical behavior and the mapping of interactively modified tissue are solved with a novel spatially and temporally adaptive space warp function.

2 BACKGROUND

In order to improve the immersion into a VE, it is beneficial to provide the user with touch feedback, as it has been shown that the presence of coherent multi-modal sensations influences task performance in a positive way (e.g. [36, 5, 31]). In keyhole surgery training simulators, user-guided instrument replicas are usually linked to haptic devices (e.g. [44, 1]), albeit active haptic feedback comes with challenging problems related to the mechanical designs and high update rates. An elegant and cost-effective alternative to active feedback is to build upon passive haptics, where a VE is combined with a corresponding physical object which provides the tactile cues [28]. Further research also showed that passive haptics can improve the feeling of presence in users [14, 13, 43, 27]. In medical education, physical mock-ups have been combined with augmented reality visualizations [22, 38]. An arthroscopic knee surgery simulator which builds upon passive haptics has been presented in [30]. The authors later showed that tactile cues induced by physical bone objects greatly affect task performance [26]. Recently, passive haptics has been combined with active components such as vibration motors in order to mimic textures and to alter the stiffness perception of materials [42, 32].

Unfortunately, a main weakness of passive haptics remains its lack of flexibility, stemming from the one-to-one mapping between the VE and the physical object. In the context of surgical training simulators, this is particularly severe, as a main benefit over pure mechanical box trainers is thought to be their variability in virtual patients. Though, there is a resort to this limitation, notably building upon *sensory illusions*. Already almost a century ago, it has been shown that users wearing distortion glasses perceive a flat surface as curved [11]. Since then, numerous studies have been conducted which investigate into the

• Jonas Spillmann is with Computer Vision Laboratory, ETH Zurich.
E-mail: jonas.spillmann@vision.ee.ethz.ch.

• Stefan Tuchschmid is with VirtaMed Inc. E-mail:
tuchschmid@virtamed.com.

• Matthias Harders is with Computer Vision Laboratory, ETH Zurich and University of Sheffield, United Kingdom. E-mail:
harders@vision.ee.ethz.ch.

Manuscript received 13 September 2012; accepted 10 January 2013; posted online 16 March 2013; mailed on 16 May 2013.

For information on obtaining reprints of this article, please send e-mail to: tvug@computer.org.

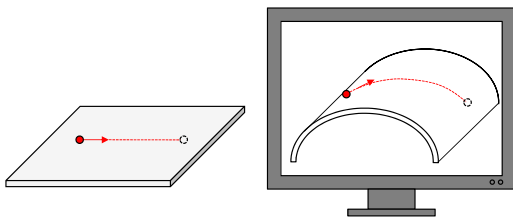


Fig. 1. Simple example of space warping: The straight linear movement of a real user-guided instrument on a flat surface (left) is mapped to a non-linear path when the plane is warped to a curved surface in the VE (right).

way how humans combine visual and haptic cues, showing that the visual channel generally dominates the haptic percept when they are in slight contradiction (see *e.g.* [35, 39, 10, 12]). In [9] and [24], it is shown that the perceived stiffness varies for virtual materials differing in elasticity, even if the force feedback is constant. In a similar notion, the speed of the mouse cursor can be modified to give the sensory illusion of a non-flat surface [23], or the position of the virtual hand can be changed to avoid visual interpenetrations in the VE [6]. The question of how much discrepancy is allowed without users being disturbed is discussed, *e.g.*, in [25, 3, 34], and in the context of augmented reality in [21].

Generally speaking, sensory illusions in this regard are a special case of a deliberate mismatching between the real and a virtual world. Other examples of such mismatching include [16] where warped mappings between a 3D control- and display-space is proposed. In [8], the limited workspace of a haptic device is enlarged in the VE. An extreme case for a deliberate mismatching is the switch of scales, *e.g.*, to manipulate molecules haptically [4]. Another intriguing application of this concept is *redirected walking*, which allows exploring a large VE in a limited physical space. This is done by scaling the rotation of the VE shown via a head-mounted display to a user [33, 19, 41].

The idea of employing sensory illusions in combination with passive haptics within surgical training simulators has first been described in [29]. They showed in a study that the perceived hardness of structures can be enhanced by their visual appearance. We build upon the previous work in [17, 20] where a generic framework for mismatching the VE with physical objects by warping the free space around the objects is proposed. This was accomplished by solving a 3D thin plate problem. This method ensured that the touching events occur simultaneously in the real space and in the VE while keeping the distortions minimal. By tracking the real finger of a user while placing the virtual representation in a warped space, a large variety of different virtual shapes can be plausibly touched [18]. A user study has also been performed to show the benefits of the method [20]. Similar in spirit is the recent work in [2] that presents a passive haptics system where the user touches a cylindrical physical object that is warped to a set of differently-shaped virtual objects. The avatar of the user's finger is displaced based on a semi-analytical space warp scheme. Similar to [20] and [2], we warp the free space inside the knee joint such that the tactile cues from differently-shaped virtual bones can be provided by one generic physical bone object. We then extend this approach such that temporally-varying and position-dependent mappings can be obtained.

3 EXAMPLE SURGICAL SIMULATOR TEST-BED

We present our approach in the scope of a prototype training simulator for knee arthroscopy. The simulator hardware contains a knee replica including bones, menisci, and ligaments (see Fig. 2). A rubber skin hides the knee interior, and adds to the stability of the knee joint.

The tibial bone can be displaced by the user, allowing for both *flexure* and *varus/valgus* opening of the knee joint; varus/valgus opening refers to an inward or outward bending of the knee joint (resulting in a knock-knee or bow-leg configuration). Bones and surgical instrument replicas are tracked, allowing to arrange the virtual models accordingly. On the software side, a high-fidelity VE including the bones, menisci, and ligaments is simulated in real-time. Both the virtual knee joint and the virtual instruments are arranged according to the tracked 6-DOF configuration of their real counterparts. The endoscopic view of the virtual arthroscope is synthesized and rendered on the screen.

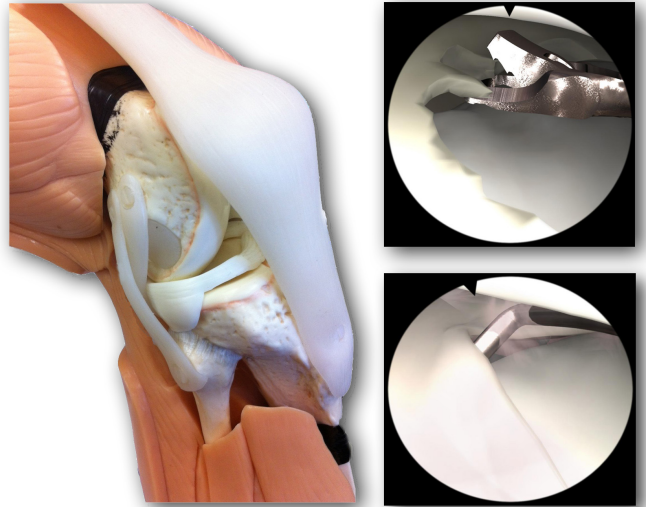


Fig. 2. The knee replica includes bones, ligaments, and menisci. The structures consist of different materials giving realistic tactile cues (the skin is not shown) (left). The virtual simulation includes deformations and interactive modifications of the meniscus (right).

4 SPACE WARPING

In this section, we describe the extension of the previous concepts [20, 2] to spatially and temporally adaptive space warping. We start by introducing the notion of mapping non-conforming virtual and physical shapes. Based on this, we show how to warp the free space surrounding these components such that a spatially smooth space warp is obtained. Finally, we propose to extend this approach to spatially and temporally adaptive space warping.

4.1 Mapping Non-conforming Surfaces

Employing passive haptics in a VE denotes that the touching event in the virtual world is simultaneously accompanied by a tactile sensation, induced by the contact between a user-guided handle and the physical environment. We assume that the user interacts with the VE through any kind of *avatar* [17], which can be a body part of the user, such as his/her finger as in [18, 2], his/her entire body [41], but also any kind of user-guided tool, as the instruments in endoscopic surgery.

For compelling passive haptics, it is crucial that the touching events in the VE and in the physical world occur concurrently. That is, whenever the physical handle touches a wall of the physical environment, the avatar must be in contact with the corresponding wall of the VE. While this is trivially ensured for conforming virtual and physical environments, warping of space is required if non-conforming virtual and physical components are considered. To accomplish this, let us first assume a function

$$\mathcal{F} : \mathbf{x} \in S \mapsto \mathbf{x}' \in S' \quad (1)$$

which provides the mapping of the surface (*i.e.*, the walls) of the VE from the shape S that corresponds to the physical objects to a desired

shape S' . The latter corresponds to the distorted VE. Note that this warp target is a central notion in our approach, which will appear in all presented techniques. The required shapes can stem from different sources, for instance medical scans, manual modeling, or computations. Based on this, we define the general *warp displacement* in a point $\mathbf{x} \in S$ as $\Delta\mathbf{x} = \mathcal{F}(\mathbf{x}) - \mathbf{x}$, which is the difference between the original and the distorted VE.

In order to ensure that the touch events in the physical environment and in the distorted VE occur simultaneously, the avatar must touch the distorted VE if and only if the user touches the physical environment. Consequently, when the surface T of an avatar touches the original surface S of the VE in a contact point $\mathbf{x}_c = S \cap T$, the avatar has actually been displaced by $\Delta\mathbf{x}_c = \mathcal{F}(\mathbf{x}_c) - \mathbf{x}_c$. That is, the entire surface T is displaced by the appropriate warp displacement $\Delta\mathbf{x}_c$, resulting in the warped avatar T' (see Fig. 3). Note that this displacement is *rigid*, based on the one-point contact between the avatar and the VE. Since surgical tools such as probes or scissors are usually rigid, this results in a more intuitive behavior. However, this could lead to interpenetrations in case of multi-contacts (see Sec. 6 for further discussions).

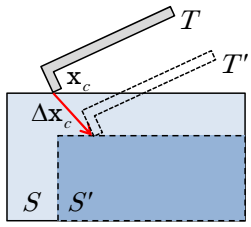


Fig. 3. In order to obtain the warped avatar T' , the avatar T is rigidly translated by the warp displacement $\Delta\mathbf{x}_c$ (red arrow) of the contact point \mathbf{x}_c .

4.2 Static Space Warp

In the previous section, we have illustrated that, given that the unwarped avatar touches the original surface, the warped avatar results from adding the warp displacement of the contact point. However, to obtain a spatially smooth movement of the warped avatar, the free space around the environment must be distorted as well, as proposed in [20, 2].

To ensure a smooth behavior, we require a C^1 -continuous function $W : \mathbb{R}^3 \rightarrow \mathbb{R}^3$, which computes for each point in space a warp displacement, subject to the boundary condition $W(\mathbf{x} \in S) = \Delta\mathbf{x}$. Unfortunately, a closed form solution to obtain W does not exist. Theoretically, we could discretize the domain of W into, *e.g.*, an Eulerian grid, and compute the resulting displacements by solving a constrained variational minimization of the warp displacements. As an alternative, [20] employed a 3D thin plate formulation to solve for smooth displacements. However, such algorithms are computationally expensive, obviating their application in temporally-varying space warping in real-time simulation. Instead, we opt for a simple approximation of W , based on the minimum distances between the avatar surface T and the environment surface S .

For our test-bed system, consider that our goal is to obtain a space warping for a virtual knee joint. That is, the environment walls comprise of the discretized surfaces of the bones, menisci, ligaments, and skin. Formally, the environment surface is clustered into N groups $S[k], k = 1..N$. For example, we refer to the environment surface of the tibial bone as $S[\text{tibia}] \subseteq S$.

In the following, we limit ourselves to exactly one pre-defined *interaction point* $\mathbf{y}_o \in T$, and compute the warp displacement in the free space with respect to this point. Thus, we first compute the minimum Euclidean distances $d_k(\mathbf{y}_o, S[k])$ between \mathbf{y}_o and the k groups $S[k]$ of the environment surface, along with the corresponding warp displacement $\Delta\mathbf{x}_c[k]$ of the closest point $\mathbf{x}_c[k] \in S[k]$, as illustrated in

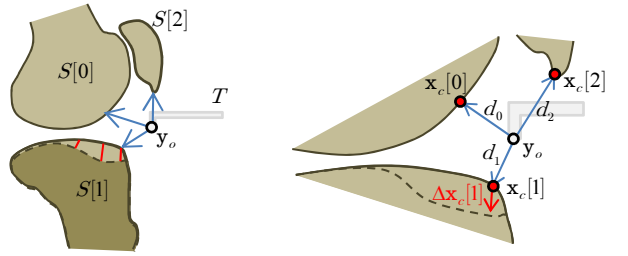


Fig. 4. Warping the free space enclosed by the knee joint for bone geometries. We compute the distances $d_k, k = 0, 1, 2$ between the interaction point $\mathbf{y}_o \in T$ and the three groups tibia, patella, and femur of the environment. The final warp displacement $\Delta\mathbf{y}_o$ is obtained by a weighted sum of the three warped displacements $\Delta\mathbf{x}_c[k]$ (left). Note that if for instance only the tibia is warped, $\Delta\mathbf{x}_c[0] = \Delta\mathbf{x}_c[2] = \mathbf{0}$ (right).

Fig. 4. The final warp displacement $W(\mathbf{y}_o)$ of the interaction point on the avatar is then obtained by a weighted sum

$$\Delta\mathbf{y}_o = \frac{\sum_{k=1}^N \omega_k \Delta\mathbf{x}_c[k]}{\sum_{k=1}^N \omega_k}, \quad (2)$$

where the weights

$$\omega_k = \exp\left(-\frac{d_k(\mathbf{y}_o, S[k])^2}{2\sigma_o}\right) \quad (3)$$

are obtained from a Gaussian kernel function, computed on the minimum Euclidean distances between \mathbf{y}_o and the environment groups $S[k]$. σ_o is the width of the kernel. Intuitively, the smaller the distance between \mathbf{y}_o and one of the surface groups $S[k]$, the smaller should be σ_o . Consequently, we set $\sigma_o = \min_k d_k(\mathbf{y}_o, S[k])$. Finally, the resulting warp displacement $\Delta\mathbf{y}_o$ is then added to all avatar points $\mathbf{y} \in T$, resulting in the warped avatar surface T' .

To summarize our basic space warping approach, we first compute the minimum distances between the interaction point \mathbf{y}_o on the original surface of the avatar and the original bone geometries. We underline that it is important to consider not only those bones which are being warped, but also the unwarped parts of the knee in order to ensure that no warping is done when the avatar touches an unwarped structure. Then, we determine the warp displacements $\Delta\mathbf{x}_c[k]$ for all structures k , based on the difference between the original and the warped surface geometries in $\mathbf{x}_c[k]$. Finally, we blend the found warp displacements $\Delta\mathbf{x}_c[k]$ in order to obtain the warp displacement $\Delta\mathbf{y}_o$, which is added to all points of the original avatar surface to obtain the warped avatar T' .

4.3 Adaptive Space Warp

In this section we elaborate how different mechanical behaviors can be realized using a parametric warping approach, again illustrated on a specific case in our test-bed simulator. When, *e.g.*, the anterior cruciate ligament (ACL) in the knee is torn, then the joint becomes more flexible. The joint in particular allows for a significantly larger valgus/varus opening (see Fig. 5). Unfortunately, the generic knee joint replica does not support this behavior; a particular opening always requires the same amount of force applied to the bone. However, we can mimic a torn ACL by employing the space warp framework.

The governing idea is based on the observation that the warped geometry S' is obtained by applying a mapping function $\mathcal{F}(\mathbf{x})$ to the original geometry S . We now redefine this function to depend on an additional scalar parameter s which controls the *amount of warping*,

$$\mathbf{x}' = \mathcal{F}(\mathbf{x}; s) \quad s \in [0, 1], \quad (4)$$

with $\mathbf{x} = \mathcal{F}(\mathbf{x}; 0)$ meaning no warping is applied. The warping is now a function depending on some variable, wherefore we refer to it as *adaptive warping*.

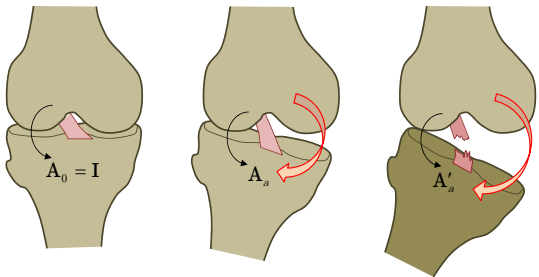


Fig. 5. Adaptive space warping in order to represent a knee with a torn ACL, and consequently a larger valgus/varus opening angle. The knee joint in the rest pose, corresponding to $\mathbf{A} = \mathbf{I}$ (left). The knee joint with the maximally valgus-opened knee is in the pose $\mathbf{A} = \mathbf{A}_a$, where the opening angle is governed by the physical model. \mathbf{A}_a is the key pose (middle). The mimicked joint opening $\mathbf{A} = \mathbf{A}'_a$ in absence of a stabilizing ACL, is the target pose \mathbf{A}'_a (right).

To realize this, consider the homogeneous transformation matrix $\mathbf{A} \in SE(3)$, which represents the position and orientation of the tibial bone with respect to its initial configuration $T_0[\text{tibia}]$, *i.e.*,

$$\begin{pmatrix} \mathbf{x} \\ 1 \end{pmatrix} = \mathbf{A} \begin{pmatrix} \mathbf{x}_0 \\ 1 \end{pmatrix} \quad \mathbf{x} \in T[\text{tibia}], \mathbf{x}_0 \in T_0[\text{tibia}] \quad (5)$$

where $\mathbf{A}_0 = \mathbf{I}$ in the *rest pose* of the knee joint. Each value of \mathbf{A} corresponds to a different pose, *i.e.*, a different joint opening.

Now, assume that the hardware knee model is in a *key pose* $\mathbf{A} = \mathbf{A}_a$ corresponding to a maximally valgus-opened knee. However, to mimic a torn ACL, the virtual knee model should instead have an even larger opening angle, which would be our *target pose* \mathbf{A}'_a (see Fig. 5). In practice, we obtain \mathbf{A}'_a by removing the ligaments from the knee replica and recording the resulting valgus-opened pose. The matrix $\Delta\mathbf{A}_a = (\mathbf{A}'_a)^{-1}\mathbf{A}_a$ corresponds to the difference between these two poses. We now define

$$\begin{pmatrix} \mathcal{F}(\mathbf{x}; s) \\ 1 \end{pmatrix} := \text{interp}(s, \mathbf{I}, \Delta\mathbf{A}_a) \begin{pmatrix} \mathbf{x} \\ 1 \end{pmatrix} \quad \mathbf{x} \in T[\text{tibia}] \quad (6)$$

that is, we interpolate between the unwarped current tibial bone geometry $T[\text{tibia}]$, and a rigidly transformed tibial bone, where $\text{interp}(\cdot)$ is an arbitrary, *i.e.*, linear or non-linear, interpolation operator. In practice, we linearly interpolate the translational part of the transformation and spherically interpolate its rotational part.

The full warping should, however, only be applied when the current pose of the physical knee approaches the key pose \mathbf{A}_a . Consequently, we let s be proportional to the difference between the current pose \mathbf{A} and the key pose \mathbf{A}_a . Due to the stiff rubber ligaments of the plastic knee model, the rotational part of \mathbf{A} dominates. Therefore, we set s based on the angular difference $\alpha = \angle(\mathbf{A}, \mathbf{A}_a) \in [-\pi, \pi]$, and employ again a Gauss kernel to obtain values between 0 and 1,

$$s = \exp\left(-\frac{\alpha^2}{2\sigma_\alpha^2}\right) \quad (7)$$

where $\sigma_\alpha = \angle(\mathbf{I}, \mathbf{A}_a)$ is the kernel width, depending on the angle between rest and key pose. This results in the desired behavior; it allows warping the virtual knee joint to the desired target pose in the VE, when the current physical pose approaches the key pose.

Note that in order to further improve the warping, it is actually beneficial to use multiple pairs $(\mathbf{A}_a, \mathbf{A}'_a)$, each corresponding to a different bending angle. For this we just define one map function $\mathcal{F}_\tau(\mathbf{x}; s_\tau)$ per pair $(\mathbf{A}_a, \mathbf{A}'_a)$, $(\mathbf{A}_b, \mathbf{A}'_b)$, etc., where s_τ represents the influence of the pair $(\mathbf{A}_\tau, \mathbf{A}'_\tau)$. During the simulation, the distance between \mathbf{y}_o and the original tibial bone in the current pose \mathbf{A} is computed and the warp displacements that depend on the distance between \mathbf{A} and each key pose \mathbf{A}_τ are assembled. In the results, we demonstrate that already three pairs are sufficient to plausibly model a torn ACL behavior.

4.4 Temporal Space Warp

Finally, we will outline how we can use space warping to even accommodate for user-controlled changes in the scene. To explain what we understand as a temporal space warp, consider a virtual patient having a damaged meniscus. The standard treatment is to remove the meniscus locally around the damaged region with a cutting instrument. This is a challenging task which is hardly possible in a simulator based on passive haptics: actual cutting of the meniscus replica is not desired since this would irreparably destroy the simulator hardware. In contrast, if the meniscus replicas are not modified, then the user will experience a haptic irritation, since he/she feels a tactile cue of the original meniscus, while the virtual meniscus has been cut-off. Again, space warping provides an elegant resort to this problem. In contrast to the basic approach, we have a temporal dependency; that is, we start with an unwarped meniscus and progressively switch to space warping, depending on the location and amount of excised meniscus tissue in the VE.

The main challenge in temporal space warping is that in each cut I , the topology of the meniscus geometry is altered, parts of the previous meniscus surface S^{I-1} are removed, and a new meniscus surface S^I is built along the intersection of the meniscus surface and the blade surface. We consider the cutting algorithm as a black box; details can be found in [40, 37]. What makes the problem more challenging than the static warp in Sec. 4.2 is that here, the warp function \mathcal{F} cannot be pre-computed or manually designed. Instead it must be determined automatically at run-time, based on the current cutting state. In theory, we could re-mesh the cut meniscus surface S^I such that it matches again the topology of the original meniscus S^0 , or likewise re-mesh the original meniscus geometry to match the current state. However, re-meshing is computationally expensive, which forbids its application in interactive simulations. A geometric projection of the original surface onto the cut surfaces does not work either, since the identification of corresponding surface features is not straightforward. Here, we propose a simple solution, which again derives the mapping function based on a prior-known target surface.

During pre-computation, a warped meniscus S'_{\max} is generated that corresponds to a maximally cut meniscus, as depicted in Fig. 6 on the left. This could for instance be done manually with a sculpting software or automatically with a statistical shape model. Then, at simulation time, the goal is to compute a blend between the original geometry S and the maximally warped geometry S'_{\max} such that the current cut meniscus geometry S^I is approximated. This is accomplished by considering both the *amount* of removed material and the *location* of the cut.

More precisely, let $V(S) \in \mathbb{R}$ be the volume enclosed by the surface S . For triangulated manifolds, this function can be evaluated efficiently. Then, V^I is the enclosed volume of the current meniscus surface after the I -th cut. Further, by comparing the topologies of S^I and S^{I-1} , we can obtain the geometry of the newly created cut surface, yielding information on location $\mathbf{x}_{\text{cut}}^I$ and geometric extent h^I of the region of excised material.

For our test-bed, we consider that the meniscus in the VE is modified by employing a punch-like cutting instrument with a volumetric blade geometry, as illustrated in Fig. 6. We adjust the amount of local blending by applying an effect similar to brush-sculpting. A modification process approximating the geometry of the blade is applied around $\mathbf{x}_{\text{cut}}^I$ with a geometric extent of h^I . In addition, we introduce a scalar s which controls the magnitude of the effect on the surface points.

Thus, we blend between the current and the maximally warped displacements in the region around $\mathbf{x}_{\text{cut}}^I$, and again resort to a Gaussian kernel to smooth out the blended displacements towards the borders of the approximated brush tool (see Fig. 6). Conceptually, this corresponds to an adaptive mapping function

$$\mathcal{F}(\mathbf{x}; \mathbf{s}) := (\mathbf{I} - \text{diag}(\mathbf{s}))\mathbf{x} + \text{diag}(\mathbf{s})\mathbf{x}'_{\max} \quad \mathbf{x} \in S, \mathbf{x}'_{\max} \in S'_{\max} \quad (8)$$

depending on the original surface S and a vector $\mathbf{s} \in \mathbb{R}^m$ of point-wise scalars, where m is the number of surface points of the discretized



Fig. 6. As a pre-computation step, a maximally-warped meniscus S'_{\max} is generated (left). During the meniscus cutting simulation, a part of the original meniscus surface S^0 is interactively removed with the punch (middle), resulting in a new surface S^1 . To adjust the warped meniscus surface, the warp displacements are blended in a brush-sculpting-tool-style, applied in the center x_{cut}^1 of the first cut region. The resulting warped meniscus surface S'^1 (dashed) is a reasonable approximation of the cut surface (right).

meniscus geometry. In order to guarantee that the difference between the two warped geometries corresponds to the amount of removed material, we perform this step iteratively in a binary search for the vector $\mathbf{s} = (s_1 \dots s_m)$ such that the volume of the warped surface matches the current volume of the cut meniscus surface (see Algorithm 1). Experiments have shown that a sufficient approximation of the target

Algorithm 1 brushWarp() // function called after each cut I

```

// initialize variables for the binary search
 $s \leftarrow \frac{1}{2}$  // start with 50% warp
 $k \leftarrow \frac{1}{4}$ 
// perform binary search for the variable  $s$  ('magnitude' of brush)
repeat
     $s^I \leftarrow s^{I-1} + \text{gaussianBrush}(x_{\text{cut}}^I, h, s)$ 
     $S'^I \leftarrow \mathcal{F}(\mathbf{x}, s^I)$  // compute the distorted geometry  $S'^I$ 
    // adjust  $s$  in order to approach the target volume  $\mathbf{V}^I$ 
    if  $V(S'^I) > V^I$  then
         $s \leftarrow s + k$ 
    else
         $s \leftarrow s - k$ 
    end if
     $k \leftarrow \frac{k}{2}$  // adjust  $k$  to refine the binary search step
until  $|V(S'^I) - V^I| < \varepsilon$ 

```

volume is reached after at most 5 iterations.

Note that the resulting warped geometry S'^I usually does not correspond exactly to the current cut meniscus geometry S^I . However, in our experiments this was not detrimental to the cutting procedure. In addition, the described approach is very robust, since the approach only relies on per-point scalars $s_i \in [0, 1]$ instead of displacements; consequently, the warping cannot diverge, even if violent, unpredicted user interactions occur. Of note is that we are currently limited to volumetric blade geometries that cut non-progressively. However, an extension to knife-like blades should be straightforward; we will address this issue in future work.

4.5 Combining the Approaches

In the previous sections, we have presented two extensions to the static space warp approach. In many cases, it is beneficial to combine these approaches, for example, to represent a knee with a torn ACL and a differing bone geometry. The combination of static space warping with adaptive space warping is straight-forward. This is because the warp displacements can be added serially, *i.e.*, we can first compute a warp displacement based on the distance between the current and the key pose of the knee joint. Then, we compute a second warp displacement, based on the distance between the unwarped avatar and the original tibia shape, and the mapping from the original tibia shape to its distorted counterpart. The first and the second warp displacement can then be simply added, where the first, adaptive warp displacement is scaled by the parameter s . The resulting distorted tibia shape is ob-

tained by transforming the statically warped tibia shape by (6), instead of the original tibia shape.

The combination of the temporal space warp with the static approach is less intuitive, since the former is always interpolated between the original and a maximally warped shape. However, it is again possible to consider the processes serially; but in this case, the order of application is important. We always compute first the static warp which maps the original to its distorted shape. By translating the avatar by this displacement, we obtain the warped avatar *and* the statically warped object. The cutting is then performed based on the warped geometries. Now, and this is different to the approach described above in Sec. 4.4, we apply the brush to the statically warped surface. Formally, the resulting map is obtained as the combination $\mathcal{G} \circ \mathcal{F}$, with

$$\mathcal{F} : \mathbf{x} \in S \rightarrow \mathbf{x}' \in S' \quad (9)$$

being the static warp and

$$\mathcal{G} : \mathbf{x}' \in S' \times \mathbf{s} \in \mathbb{R}^n \rightarrow \mathbf{x}'' \in S'' \quad (10)$$

the temporal warp, interpolating between the uncut but statically warped object S' and the maximally cut warped object S'_{\max} , and resulting in the correctly warped shape S'' .

5 RESULTS

In this section, we show how the presented methods integrate into a prototype of a training simulator for knee arthroscopy. We focus on the core message of our paper, notably that the concept of sensory illusions in the context of passive haptics can be employed to simulate different virtual patients on one generic hardware.

5.1 Differing Bone Geometries

We employ the basic space warping approach to represent a wide variety of different knee geometries on one generic hardware. An example use-case is a knee with *arthrosis*, *i.e.*, a degeneration of the tibial cartilage which results in an erosion of the cartilage. As starting point, we have taken a 3d-scan of the tibial bone replica. We have then manually deformed the virtual bone geometry in order to represent the cartilage erosion. Since the deformation is purely geometric and maintains the topology, the correspondence \mathcal{F} is obtained trivially. In Fig. 7 on the left, both the original tibia surface (top) and the displaced tibia surface (bottom) are shown. For demonstration purposes, we have modeled a highly exaggerated cavity with a depth of 0.3cm. The two middle images in Fig. 7 show the simulated camera image without and with the arthrosis. The palpation hook is correctly warped such that in both cases, a tactile cue from the hardware tibia bone is provided when its avatar is in contact with the bone. In Fig. 7 on the right, we have moved the hook on a straight line about 0.1cm above the tibial plateau. The green line corresponds to the case without space warp, the red line corresponds to the warped path. Clearly visible is the distortion in the region of the cavity resulting from the space warp. One of the main benefits of our approach is that our approximation of the space warp function W does not require any pre-computation, and that it can be evaluated efficiently at run-time. The average time to warp the palpation hook is as few as 0.1ms.

5.2 Torn Ligaments

In order to represent virtual patients with torn ligaments, we have proposed to let the amount of space warping depend on some scalar. By letting this scalar correspond to the distance between the current knee configuration and a target configuration, we can mimic a larger opening angle than provided by the hardware knee model. To illustrate this, we use three pairs of key and target poses; at 15°, 45°, and 65° bending angle, respectively.

For each pair, we then obtain the target pose by removing the rubber ligaments from the knee replica. Fig. 8 illustrates the rest pose of the knee model and the key pose for the 45° bending angle. The violet overlay shows the target pose without ligaments, the angular difference $\angle(\mathbf{A}_a, \mathbf{A}'_a)$ between the key and the target pose is about 10°. In

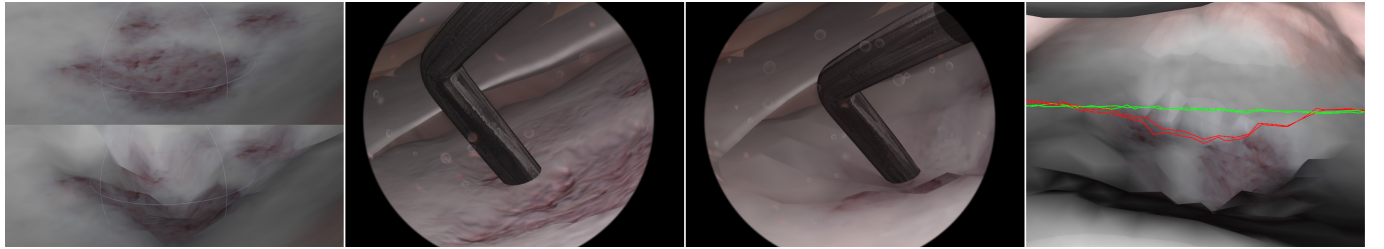


Fig. 7. The static space warp technique is employed to represent a tibial bone with arthrosis. The arthrosis results in a cavity of about 0.3cm depth (left). The rendered camera images, without and with warping (middle left and right). The movement of the hook on a straight line path results in a straight line (green) in absence of space warp, which is distorted (red) when space warping is employed (red).

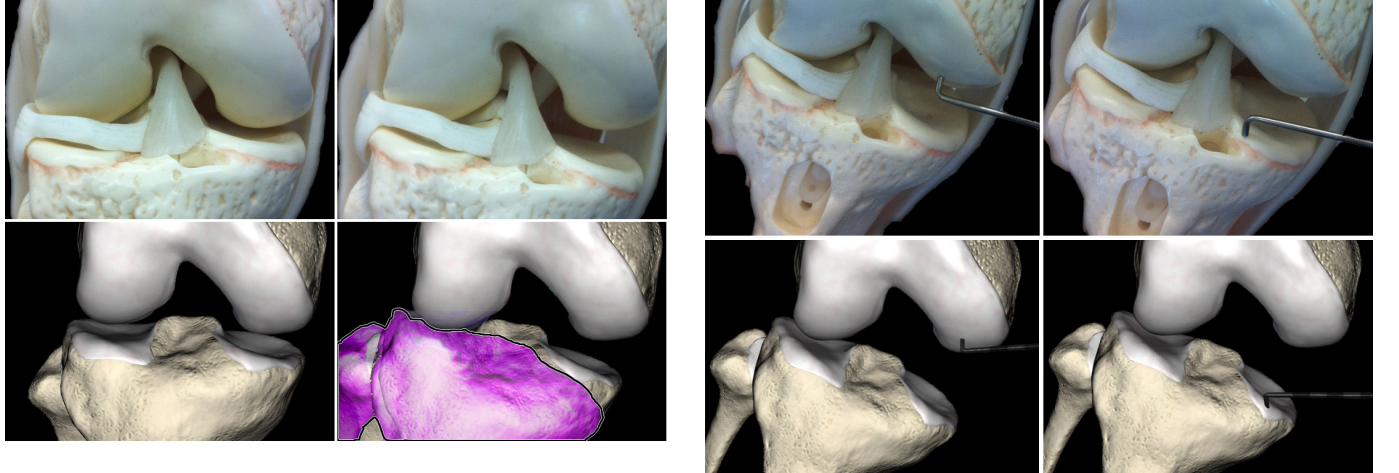


Fig. 8. The knee replica (top) and the virtual model (bottom) in the rest pose (left), and in a valgus-opened pose. The violet overlay corresponds to the target pose of the tibia (right).

the simulation, the adaptive space warping is then employed to plausibly mimic the mechanical behavior. The touch events occur simultaneously, as illustrated in Fig. 9.

To illustrate the course of the valgus-opening for a continuous bending of the knee joint, we valgus-opened the knee joint maximally (the maximum valgus-opening is governed by the knee hardware), and plot the superimposed valgus angles for various bending angles. The experiment is repeated for three pre-defined key values, for only one pre-defined key value, and without adaptive warping. The curves in Fig. 10 illustrate that the course of the superimposed valgus-opening is already very smooth if three key values are employed. In the case of only one key value, the curve exhibits a spike around the value, and goes down to its unwarped value for configurations further away.

5.3 Meniscectomy

Meniscectomy denotes the removal of damaged parts of the knee menisci. In this operation, the meniscus tissue is removed with a punch around the damaged region (see Fig. 6). However, the interactive modification of tissue is challenging in the context of passive haptics, since the physical object must not be modified. We show that by employing our method, we can maintain the tactile cues induced by the elastic physical meniscus replica. At simulation, the user drives the punch blade to the meniscus, and cuts off a piece of the meniscus. The cut-off piece is then washed off. It is then spatially blended between the original and the maximally cut meniscus, based on the amount and on the location of the cut. In Fig. 11, the process is illustrated. The leftmost image shows the simulated camera image. The other three images show the meniscus before the first cut, after the first cut, and after 15 cuts. The red lines correspond to the determined warp displacements. The volume of the current meniscus $V(S^1)$ is 2.360cm^3 , and the volume $V(S'^1)$ of the warped meniscus is 2.358cm^3 . However,

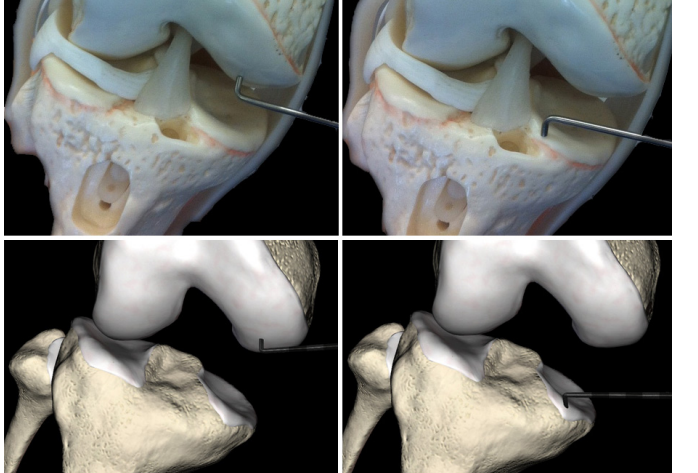


Fig. 9. Our space warping approach guarantees that touch events occur simultaneously in the physical (top) and in the virtual (bottom) environment.

the computation of the per-point scalars s_i in the interactive cutting (Algorithm 1) is expensive and takes for this scenario about 3.8ms on average. However, the computation only needs to be done once after each cut.

6 DISCUSSION

We have proposed to employ a spatially and temporally adaptive space warping approach in order to represent virtual knee models with differing opening behaviors and to handle interactive modifications of the virtual tissue. The key of our method is efficient approximations of both the mapping function \mathcal{F} and the space warp function W . However, a number of limitations and caveats exist which we discuss below.

First, our approach is currently limited to one pre-defined interaction point y_o . That is, the warp displacement of the avatar is always computed with respect to y_o , and not to the actual contact point. Consequently, minor interpenetration artifacts might occur in case of a large distance between y_o and x_c . In theory, it would be possible to compute the minimum distances between all points $y_i, i = 1..n$ and the N environment surface groups $x[k]$. Then, we could warp each y_i individually with the obtained warp displacements Δy_i . However, the resulting approach would not only be computationally expensive, but also the resulting warp of the avatar would, in general, not be rigid. It would depend on the curvature of the imposed space warp field around the avatar. In turn, this would result in a rather unnatural behavior of an apparently rigid instrument. Another possibility would be to choose the interaction point y_o dynamically, based on the anticipated contact point between the avatar and the environment. However, it would be challenging to guarantee the temporal continuity of the resulting warp. Still, we will address this issue as future work. We also point out that the limitation to one interaction point only leads to minor artifacts for

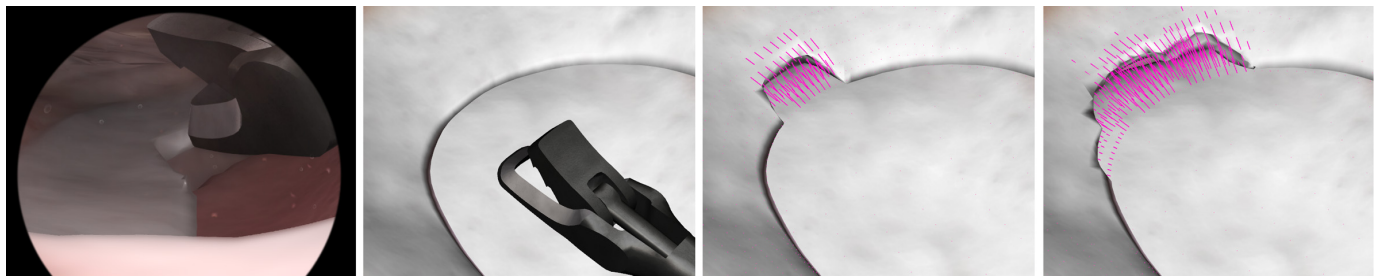


Fig. 11. Automatic computation of the warped mesh in interactive meniscus cutting. The images show the simulated VE (left), and the meniscus before the first cut, after the first cut, and after 15 consecutive cuts. The purple lines illustrate the interactively computed warp displacements.

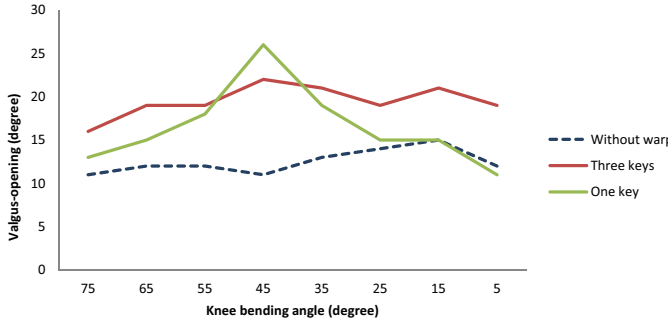


Fig. 10. Course of the maximum valgus-opening for various flexing angles, by employing no, one (45°) or three (65° , 45° , 15°) key values. Clearly visible is the spike around 45° when only one key value is employed. Already three key values result in a sufficiently smooth valgus-opening course.

strongly curved space warp fields and large distances between the contact and the interaction point.

Second, we have proposed to approximate the space warp function W by computing the minimum distances between \mathbf{y}_o and the N environment clusters $S[k]$ corresponding to the bones and soft structures in the case of the knee joint. To verify that the approximation (2) is fair, consider the situation where the avatar is exactly in the middle of the free space enclosed by the environment. In this case, $\Delta\mathbf{y}_o$ contains a mix of equally weighted warp displacements of the nearby environment surfaces. When now the avatar is moved towards one particular surface group $S[k]$, the influence of the corresponding closest-point warp displacement $\Delta\mathbf{x}_c[k]$ grows continuously, while the kernel width of the Gauss kernel (3) shrinks, resulting in the warp displacements of the other groups being blended out. If, in contrast, the avatar is moved tangentially on the environment surface, then the resulting warp displacement $\Delta\mathbf{y}_o$ always corresponds to that of the contacted surface. That means, as long as the map function \mathcal{F} is spatially continuous, $\Delta\mathbf{y}_o$ will also change continuously. The only situation where we might encounter a discontinuous jump of $\Delta\mathbf{y}_o$ is when the obtained closest point $\mathbf{x}_c[k]$ changes. However, this situation can be avoided by only employing convex groups $S[k]$, at least for those groups which have warp displacements $\|\Delta\mathbf{x}_c \in S[k]\| > 0$.

Third, the proposed approach to handle interactive modifications has some drawbacks, which require additional effort to be overcome. First, the warp field is updated instantaneously, the tool will 'jump into' the cut-off region. While this is a current limitation of the approach, it does not affect the sensory illusion in the training simulator, because it is not possible to handle the scissor without moving the instrument, that is, the instrument is anyway displaced during the cut. Second, the space warp is limited to the pre-defined maximally cut meniscus; any cuts that exceed this limit will not be covered by the space warp. Likewise, cuts that alter the genus of the surface cannot be handled properly. In both cases, the tactile cues induced by the meniscus replica would not match the scene in the VE. However, this

is not as severe as it appears to be; since the menisci are elastic structures, a visual interpenetration of the avatar in case of an absent tactile cue can be avoided in the simulation simply by deforming the virtual meniscus.

We have presented the adaptive space warping in the context of a knee arthroscopy surgical simulator where the surgeon operates with hand-held rigid instruments. The concept can easily be extended to other settings, *e.g.*, where the avatar corresponds to a finger of the user as in [20]. However, depending on the amount of space warping, it would be more difficult to maintain the user's suspense of disbelief.

7 CONCLUSION

Combining a VE with passive haptics provides an efficient and cost-effective alternative to active haptics. However, geometrically varying virtual objects are generally difficult to accommodate. In this paper, we have shown that this limitation can be overcome by building upon the concept of sensory illusions, *i.e.*, by distorting the free space around objects. In doing so, we can map different virtual objects onto one physical reality. The core of our technique is the mapping function \mathcal{F} that maps the original onto the distorted surface geometry, and allows to obtain the warp displacement per point of the original surface. Then, we compute the distances between the user-guided instrument and the surfaces of the VE, and blend the corresponding warp displacements. We have illustrated how this method can be extended to represent differing mechanical behaviors of the VE, and even interactively modified virtual objects. The presented techniques have been integrated into a prototype training simulator for knee arthroscopy. This allowed us to simulate different virtual patients on one generic knee hardware.

The concept of space warping in the context of passive haptics has further potential in virtual reality; but still several open research questions remain. For example, our method to warp the space upon modifying the tissue is only approximate. In future work, we will investigate into a more precise method to map the original meniscus surface onto the topologically modified one, which should also be capable of handling progressive cutting. In addition, we plan to carry out a user study in order to determine the limits of the suspension of disbelief, and to quantify the impact of the space warping onto the training effect.

ACKNOWLEDGMENTS

This work has been supported by the Swiss CTI project RapidPRO 12668.1 PFLS-LS.

REFERENCES

- [1] M. Agus, A. Giachetti, E. Gobbetti, G. Zanetti, A. Zorcolo, B. Picasso, and S. Franceschini. A haptic model of a bone-cutting burr. *Studies in Health Technology and Informatics*, pages 4–10, 2003.
- [2] Y. Ban, T. Kajinami, T. Narumi, T. Tanikawa, and M. Hirose. Modifying an identified curved surface shape using pseudo-haptic effect. In *Proc. IEEE Haptics Symposium*, pages 211–216, 2012.
- [3] F. Barbagli, K. Salisbury, C. Ho, C. Spence, and H. Tan. Haptic discrimination of force direction and the influence of visual information. *ACM Transactions on Applied Perception (TAP)*, 3(2):125–135, 2006.

- [4] A. Bolopion, B. Cagneau, D. Haliyo, and S. Régnier. Analysis of stability and transparency for nanoscale force feedback in bilateral coupling. *Journal of Micro-Nano Mechatronics*, 4(4):145–158, 2008.
- [5] M. Boshra and H. Zhang. Use of tactile sensors in enhancing the efficiency of vision-based object localization. In *Multisensor Fusion and Integration for Intelligent Systems*, pages 243–250. IEEE, 1994.
- [6] E. Burns, S. Razzaque, A. Panter, M. Whitton, M. McCallus, and F. Brooks Jr. The hand is slower than the eye: A quantitative exploration of visual dominance over proprioception. In *Proc. IEEE Virtual Reality*, pages 3–10, 2005.
- [7] T. Coles, D. Meglan, and N. John. The role of haptics in medical training simulators: A survey of the state-of-the-art. *IEEE Transactions on Haptics*, (99):1–1, 2011.
- [8] L. Dominjon, A. Lecuyer, J. Burkhardt, G. Andrade-Barroso, and S. Richir. The bubble technique: Interacting with large virtual environments using haptic devices with limited workspace. In *World Haptics*, pages 639–640, 2005.
- [9] W. Durfee, C. Hendrix, P. Cheng, and G. Varughese. Influence of haptic and visual displays on the estimation of virtual environment stiffness. In *Proc. ASME Dyn Syst Control Div*, page 139144, 1997.
- [10] M. Ernst and M. Banks. Humans integrate visual and haptic information in a statistically optimal fashion. *Nature*, 415(6870):429–433, 2002.
- [11] J. Gibson and M. Radner. Adaptation, after-effect and contrast in the perception of tilted lines. i. quantitative studies. *Journal of Experimental Psychology*, 20(5):453, 1937.
- [12] H. Helbig and M. Ernst. Optimal integration of shape information from vision and touch. *Experimental Brain Research*, 179(4):595–606, 2007.
- [13] H. Hoffman. Physically touching virtual objects using tactile augmentation enhances the realism of virtual environments. In *Proc. Virtual Reality Annual International Symposium*, pages 59–63, 1998.
- [14] H. Hoffman, J. Groen, S. Rousseau, A. Hollander, W. Winn, M. Wells, and T. Furness. Tactile augmentation: Enhancing presence in virtual reality with tactile feedback from real objects. *American Psychological Society*, 1996.
- [15] B. Insko. *Passive haptics significantly enhances virtual environments*. PhD thesis, University of North Carolina, 2001.
- [16] J. Keijser, S. Carpendale, M. Hancock, and T. Isenberg. Exploring 3d interaction in alternate control-display space mappings. In *IEEE Symposium on 3D User Interfaces*, 2007.
- [17] L. Kohli. Exploiting perceptual illusions to enhance passive haptics. In *Proc. of IEEE VR Workshop on Perceptual Illusions in Virtual Environments*, pages 22–24, 2009.
- [18] L. Kohli. Redirected touching: Warping space to remap passive haptics. In *IEEE Symposium on 3D User Interfaces*, pages 129–130. IEEE, 2010.
- [19] L. Kohli, E. Burns, D. Miller, and H. Fuchs. Combining passive haptics with redirected walking. In *Proc. Augmented tele-existence*, pages 253–254. ACM, 2005.
- [20] L. Kohli, M. Whitton, and F. Brooks. Redirected touching: The effect of warping space on task performance. In *IEEE Symposium on 3D User Interfaces*, pages 105–112. IEEE, 2012.
- [21] E. Kwon, G. Kim, and S. Lee. Effects of sizes and shapes of props in tangible augmented reality. In *IEEE International Symposium on Mixed and Augmented Reality*, pages 201–202, 2009.
- [22] R. Lapeer, M. Chen, and J. Villagran. An augmented reality based simulation of obstetric forceps delivery. In *IEEE and ACM Intl. Symposium on Mixed and Augmented Reality*, pages 274–275, 2004.
- [23] A. Lécuyer, J. Burkhardt, and L. Etienne. Feeling bumps and holes without a haptic interface: the perception of pseudo-haptic textures. In *Proc. SIGCHI conference on Human factors in computing systems*, pages 239–246, 2004.
- [24] A. Lécuyer, S. Cuquillart, and P. Coiffet. Simulating haptic information with haptic illusions in virtual environments. Technical report, DTIC Document, 2001.
- [25] Y. Matsuoka, S. Allin, and R. Klatzky. The tolerance for visual feedback distortions in a virtual environment. *Physiology & behavior*, 77(4):651–655, 2002.
- [26] A. McCarthy, L. Moody, A. Waterworth, and D. Bickerstaff. Passive haptics in a knee arthroscopy simulator: is it valid for core skills training? *Clinical orthopaedics and related research*, 442:13, 2006.
- [27] M. Meehan, B. Insko, M. Whitton, and F. Brooks Jr. Physiological measures of presence in stressful virtual environments. In *ACM Transactions on Graphics*, volume 21, pages 645–652, 2002.
- [28] P. Milgram and F. Kishino. A taxonomy of mixed reality visual displays. *IEICE Trans. on Information and Systems*, (12):1321, 1994.
- [29] L. Moody, A. Waterworth, J. Arthur, A. McCarthy, P. Harley, and R. Smallwood. Beyond the visuals: tactile augmentation and sensory enhancement in an arthroscopy simulator. *Virtual Reality*, 13(1):59–68, 2009.
- [30] L. Moody, A. Waterworth, A. McCarthy, P. Harley, and R. Smallwood. The feasibility of a mixed reality surgical training environment. *Virtual Reality*, 12(2):77–86, 2008.
- [31] B. Petzold, M. Zaeh, B. Faerber, B. Deml, H. Egermeier, J. Schilp, and S. Clarke. A study on visual, auditory, and haptic feedback for assembly tasks. *Presence: Teleoperators & Virtual Environments*, 13(1):16–21, 2004.
- [32] N. Phoolchund, Y. Tenzer, B. Davies, and F. Rodriguez y Baena. Extracting material stiffness from the vibration signal of an arthroscopic hooked probe. In *Annual Conference of The International Society for Computer Assisted Orthopaedic Surgery*, 2011. accepted.
- [33] S. Razzaque, Z. Kohn, and M. Whitton. Redirected walking. In *Proc. EUROGRAPHICS*, pages 289–294, 2001.
- [34] G. Robles-De-La-Torre and V. Hayward. Force can overcome object geometry in the perception of shape through active touch. *Nature*, 412(6845):445–448, 2001.
- [35] I. Rock and J. Victor. Vision and touch: An experimentally created conflict between the two senses. *Science*, 143(3606):594–596, 1964.
- [36] L. Schultz and J. Petersik. Visual-haptic relations in a two-dimensional size-matching task. *Perceptual and motor skills*, 78(2):395–402, 1994.
- [37] M. Seiler, D. Steinemann, J. Spillmann, and M. Harders. Robust interactive cutting based on an adaptive octree simulation mesh. *The Visual Computer*, pages 1–11, 2011.
- [38] T. Sielhorst, T. Obst, R. Burgkart, R. Riener, and N. Navab. An augmented reality delivery simulator for medical training. In *International Workshop on Augmented Environments for Medical Imaging-MICCAI Satellite Workshop*, volume 141, 2004.
- [39] M. Srinivasan, G. Beauregard, and D. Brock. The impact of visual information on the haptic perception of stiffness in virtual environments. In *ASME Winter Annual Meeting*, volume 58, pages 555–559, 1996.
- [40] D. Steinemann, M. Harders, M. Gross, and G. Szekely. Hybrid cutting of deformable solids. In *Proc. IEEE Virtual Reality*, pages 35–42, 2006.
- [41] F. Steinicke, G. Bruder, T. Ropinski, and K. Hinrichs. Moving towards generally applicable redirected walking. In *Proc. Virtual Reality International Conference*, pages 15–24, 2008.
- [42] Y. Tenzer, D. B.L., and F. Rodriguez y Baena. Investigation into the effectiveness of vibrotactile feedback to improve the haptic realism of an arthroscopy training simulator. In *Studies in health technology and informatics*, volume 132, pages 517–522, 2008.
- [43] Y. Wang and C. MacKenzie. The role of contextual haptic and visual constraints on object manipulation in virtual environments. In *Proc. SIGCHI conference on Human factors in computing systems*, pages 532–539, 2000.
- [44] R. Webster, D. Zimmerman, B. Mohler, M. Melkonian, and R. Haluck. A prototype haptic suturing simulator. *Studies in health technology and informatics*, pages 567–569, 2001.